energies

MDPI

Article

Condensation of Hydrocarbons in Compact Smooth and Microfinned Tubes

Ehsan Allymehr [1,*], Ángel Álvarez Pardiñas [2], Trygve Magne Eikevik [1] and Armin Hafner [1]

[1] Department of Energy and Process Engineering, NTNU Norwegian University of Science and Technology, Kolbjørn Hejes vei 1D, 7491 Trondheim, Norway; trygve.m.eikevik@ntnu.no (T.M.E.); armin.hafner@ntnu.no (A.H.)
[2] SINTEF Energy Research, Kolbjørn Hejes vei 1, 7491 Trondheim, Norway; angel.a.pardinas@sintef.no
* Correspondence: ehsan.allymehr@ntnu.no

Abstract: A database for flowing condensation of three hydrocarbons, namely propane (R290), isobutane (R600a), and propylene (R1270), is extended by experimental tests in a smooth tube and two microfinned tubes with an increase of heat exchange area of 1.51 and 2.63, respectively. The outer diameter for all of the test tubes was 5 mm. Heat transfer coefficient and pressure drop are compared between the fluids and tubes. Tests were conducted at saturation temperatures of 35 °C and mass fluxes between 200 to 500 kg m^{-2} s^{-1}. Results show that isobutane (R600a) has a higher heat transfer coefficient and pressure drop while propylene (R1270) and propane (R290) present very similar characteristics. Both microfinned tubes increase the heat transfer coefficient compared to the smooth tube, but with different magnitude and tendencies and almost independently of the fluid tested. The maximum increase of heat transfer coefficient reached values of up to 1.8 while the maximum increase in pressure drop was by a factor of 1.7. Data have been compared with predictive methods exhibiting accurate correlation for smooth tube, while the accuracy of results for the microfinned are dependent on the type of tube and fluid used.

Keywords: hydrocarbon; refrigeration; heat transfer; pressure drop; microfinned

Citation: Allymehr, E.; Pardiñas, Á.Á.; Eikevik, T.M.; Hafner, A. Condensation of Hydrocarbons in Compact Smooth and Microfinned Tubes. *Energies* **2021**, *14*, 2647. https://doi.org/10.3390/en14092647

Academic Editor: Andrej Kitanovski

Received: 17 March 2021
Accepted: 29 April 2021
Published: 5 May 2021

1. Introduction

The refrigeration industry has been challenged by its effect on the environment. This problem is exacerbated by the current generation of working fluids that have an exceptionally high Global Warming Potential (GWP). The progress toward a more sustainable and environmentally friendly refrigeration industry requires a broad shift in the utilized working fluids to have a low GWP and zero Ozone Depletion Potential (ODP). Additionally, systems working with novel working fluids need to be more energy-efficient to reduce the indirect impact with lower primary energy usage. Propane (R290), isobutane (R600a), and propylene (R1270) have long been used as working fluids in various applications. For example, isobutane (R600a) is the most used refrigerant in domestic refrigeration and freezer units, especially in Europe [1]. Hydrocarbons offer favorable saturation curves befitting different use cases while enjoying low GWP and zero ODP. However, the use of hydrocarbons in refrigeration systems has been long limited by flammability concerns. While risk analysis has been performed on these systems showing that with careful installation, reaching the lower flammability limit is improbable [2], concerns remain. Studies have shown that the main amount of charge is stored in heat exchangers [3,4], thus minimizing the heat exchangers' volume seems to be the most effective method of increasing the capacity of these systems with regard to limitations on their charge. This is even more critical in the condenser's case as it could contain 50% of the total charge [4].

Thonon [5] and more recently Moreira et al. [6] have reviewed the literature on two-phase characteristics of flowing hydrocarbons, noting the scarcity of data available from independent laboratories for system design such as HTC and pressure drop. Moreover, the

available data seem to only focus on smooth tubes, and internally enhanced tubes are not studied. Authors are only aware of Nan and Infante Ferreira [7] where evaporation and condensation of propane in a smooth, microfinned, and crosshatched tubes with an outer diameter (d_o) of 9.52 mm were studied, showing that HTC increase is more noticeable at higher mass fluxes and experimental data are significantly over-predicted by correlations for internally enhanced tubes.

Macdonald and Garimella [8] studied condensation of propane in two tubes with internal diameter (d_i) of 14.45 mm and 7.75 mm in a broad range of saturation temperature, showing that HTC is slightly dependent on diameter while the effect of saturation temperature is much more pronounced on pressure drop. The same authors utilized the obtained data to develop HTC and pressure drop correlations [9]. Lee et al. [10] studied the condensation of three hydrocarbons, namely, R290, R1270, and R600a comparing them to R22 in smooth tubes with d_i of 12.7 and 9.52 mm. Authors noted that HTC of hydrocarbons was higher by at least 31% compared to R22, while their pressure drop was larger by at least 50%.

Del Col et al. [11] studied the condensation of R290 in a microchannel with an internal bore of 0.96 mm, showing a satisfactory agreement with the predictive methods. Ağra and Teke [12] reported experimental results for condensation of R600a in a smooth tube with d_i of 4 mm, observing that the flow was in annular form. The authors in Qiu et al. [13] simulated the condensation of R290 in minichannels with diameters ranging from 0.5 to 2 mm, visualizing the different flow patterns and the effect of flow on heat transfer and pressure drop characteristics. In another numerical study by Wen et al. [14], authors have compared condensation performance of R1234ze(E), R134a, and R290 in a tube with d_i of 1.0 mm, reporting that R290 had a lower tendency to be stratified at lower vapor qualities.

Longo et al. [15] studied the condensation of R404A and compared them to suitable hydrocarbon substitutes, namely, R290 and R1270, reporting that the hydrocarbons generally had a higher HTC while the pressure drop was lower compared to R404A, thus proving themselves to be promising candidates as a long term substitute. In a later publication Longo et al. [16], the same authors included data for R600a, noting that, while R600a has a higher HTC, its pressure drop is much higher.

The effect of internally enhanced tubes on the condensation characteristics of various working fluids has been researched in several papers. Colombo et al. [17] reported two phase flow characteristics for R134a in one smooth and two microfinned tubes while Bashar et al. [18] studied condensation of R1234yf inside smooth and microfinned tubes with d_o of 2.5 mm, showing that the HTC increase in microfinned tube can be up to 3.85 times. Diani et al. [19] compared the condensation of R513A in a smooth tube with d_i of 3.5 mm to a microfinned tube with d_i of 3.4 mm, showing that the HTC can be up to 4.5 times higher in the microfinned tube in lower mass fluxes, while, at higher mass fluxes, this increase tends asymptotically towards the increase in the heat transfer area provided by the fins. Condensation of R134a, R22, and R410A in microfinned tubes with d_i ranging between 8.92 to 4 mm was studied by Han and Lee [20] showing enhancement of HTC and penalization in the pressure drop having the same tendencies with increases in mass flux and vapor quality. The authors proposed a new correlation for the prediction of pressure drop and HTC.

Thus, while there have been several studies on the characteristics of condensation of hydrocarbons in smooth tubes, and others have analyzed the effect of internally enhanced tubes on different fluids, there have not been any studies on hydrocarbons combined with the effect of internal surface enhancement. Moreover, it seems that the comparison between different types of microfinned tubes is not available. Allymehr et al. [21,22] studied the evaporation of hydrocarbons in smooth and two microfinned tubes, demonstrating a high increase in the HTC with minimal increase in the pressure drop. As the amount of charge in the condenser is higher than in the evaporator, any charge reduction in condensers will have a higher impact. Finally, it is crucial to have reliable experimental data to properly design and size heat exchangers, especially in applications where the amount of charge is

limited by regulations. Since no experimental data are available to examine the correlations' accuracy, the predictive method's can be unreliable.

This study expands the database on condensation characteristics of R290, R600a, and R1270 in smooth and internally enhanced tubes by experimental determination of HTC and measurement of pressure drop. Two-phase flow characteristics of two microfinned tubes with different internal geometries were compared to a smooth tube at similar conditions. One of the microfinned tubes represents a more conventional internally enhanced geometry, with an increased surface area of 1.51, while the other tube has a more aggressive increase in internal surface area of 2.63. All three tested tubes have an outer diameter of 5 mm. Mass fluxes ranged from 200 to 500 kg m^{-2} s^{-1}, and results were compared with relevant correlations to review the prediction methods' accuracy.

2. Experimental Setup

The experimental test rig was previously used to measure evaporation characteristics and thus documented in Allymehr et al. [21,22]. As shown in Figure 1, the test rig was modified to allow condensation tests. The setup has two loops, one for the refrigerant and one for the secondary cooling fluid. In the refrigerant circuit, the test fluid is circulated through the system by a gear pump and mass flow is measured downstream of the pump by a Coriolis mass flow meter. The energy required to vaporize the fluid to a desired vapor quality is calculated based on measurement of pressure and temperature upstream and the temperature downstream of the preheater. This energy is provided to the fluid by the preheater by means of electrical heating tape controlled by pulse wave modulation (PWM). There is an adiabatic calming section of 75 mm upstream of the test section. A differential pressure transducer directly measures the pressure drop by pressure taps before and after the test section, located 547 mm away from each other. The average wall temperature is obtained by two pairs of thermocouples brazed to the tube wall, which are located 100 mm from the inlet and outlet of the heated test section. Thermocouples are attached to test tube's outer wall using silver brazing in a way that in each pair one thermocouple is in contact with the top and the other with the bottom part of the tube. Length of the heated section for all the tested tubes is 500 mm. Two absolute pressure sensors connected to the test section using the same pressure taps as for the differential pressure transducer provide the average value of saturation pressure at the test section, which is then used to determine the fluid saturation temperature. As the saturation pressure of R600a at 35 °C is considerably different from R1270 and R290, a different set of pressure sensors was used. Heat is removed from the test section by distilled water flowing through a helical tube wound around the test section. The helical tube geometry for water loop was optimized utilizing Ansys Fluent simulation with the goal of maximizing the temperature difference between the inlet and outlet to lower the measurement uncertainty while providing a uniform heat flux. The condensation was simulated by imposing a heat transfer coefficient and a saturation temperature while the tube diameter and length were varied at different water mass flows. The internal diameter for the cooling water tube was 4.9 mm with a length of 950 mm. The space between the helical tube for secondary fluid and the test tube is filled with melted tin. Silver brazing used for thermocouples ensures contact between the tube and the thermocouples as silver has a higher melting temperature than tin. The water temperature is measured before and after the test section using two RTD elements. Using the temperature difference, the specific heat capacity and water's mass flow, the heat removed from the test section can be calculated. Based on the results from the numerical simulation and uncertainty analysis, the water flow rate was roughly around 1180 mL min^{-1}. The heat flow to the test section is controlled by the temperature of water thermostatic bath through a PID controller. The set point for the PID was a heat flow of 155 W, thus giving a temperature change of around 2 °C. A photograph of one of the test sections is shown in Figure 2, while the schematic of the water cooling loop is visualized in Figure 3.

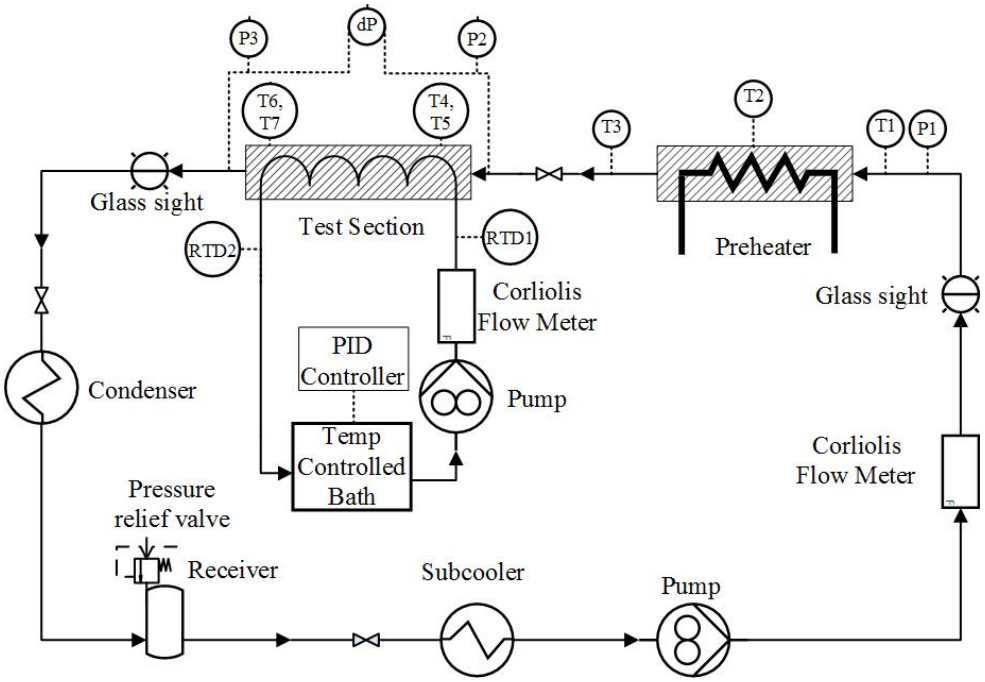

Figure 1. Test rig schematic.

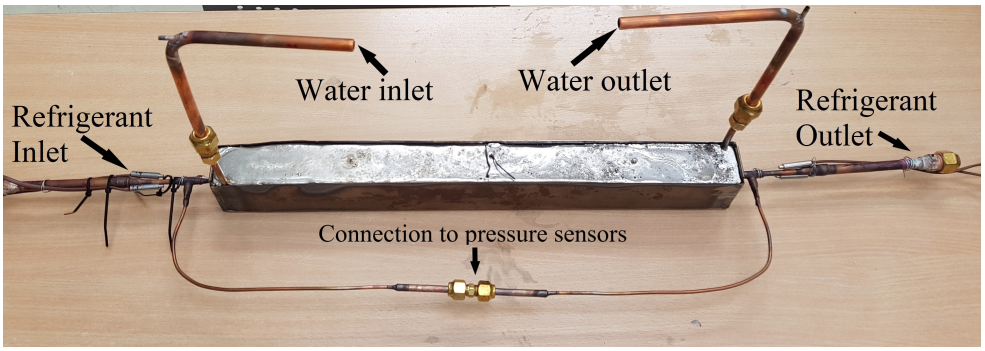

Figure 2. Photograph of one of test sections.

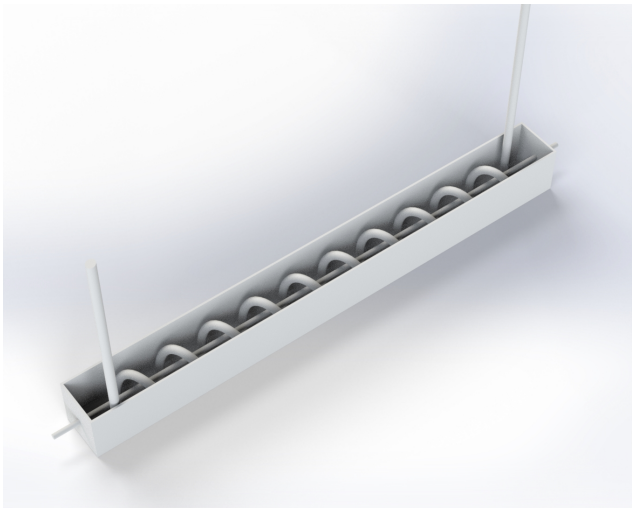

Figure 3. Visualization of test section and the cooling water loop without the filling material.

The sight glasses do not have the same diameter as the tube and therefore cannot be used for reliable detection of flow patterns. The setup is capable of quick test section changes without vacuuming the entire test rig utilizing the valves located upstream and

downstream of the test section. Before introducing new working fluids, the whole test rig is purged with nitrogen and vacuumed. The condenser and the subcooler are both plate heat exchangers. The subcooler and the condenser are connected to two separate chillers, providing a liquid flow to the pump. The condenser is located at the lowest point of the system and has the lowest temperature in the system so that it can control the system's saturation pressure by the thermal bath's temperature connected to the condenser.

2.1. Tested Tubes

One smooth tube and two internally enhanced tubes, all with an outer diameter d_o of 5 mm, were studied. Table 1 reports geometrical parameters for the tubes. Physical representations of geometrical parameters are presented in Figure 4. While the fin dimensions for the two microfinned tubes are approximately the same, MF2 has a higher number of fins and spiral angle, leading to a higher available area for heat transfer. A cross-sectional view of the two tested microfinned tubes is shown in Figure 5.

Table 1. Geometrical parameters of the test tubes.

	Unit	Smooth Tube	MF1	MF2
Outer diameter (d_o)	mm	5	5	5
Internal diameter [a] (d_i)	mm	4.1	4.32	4.26
Wall thickness [b] (t_w)	mm	0.45	0.22	0.22
Actual cross sectional area	mm^2	13.2	15.7	14.8
Effective diameter [c]	mm	-	4.47	4.34
Fin height (l_f)	mm	-	0.12	0.15
Fin number (n)	-	-	35	56
Fin angle (γ)	°	-	35	15
Spiral angle (β)	°	-	15	37
Heat exchange area ratio (R_x)	-	1	1.51	2.63
Heated test section length	mm	500		
Pressure drop measurement length	mm	547		
Test section length	mm	1005		

[a] Internal diameter for smooth tube, fin tip diameter for microfinned tubes. [b] Length between fin root and outer diameter. [c] Equivalent diameter for a smooth tube to have the same actual cross section area.

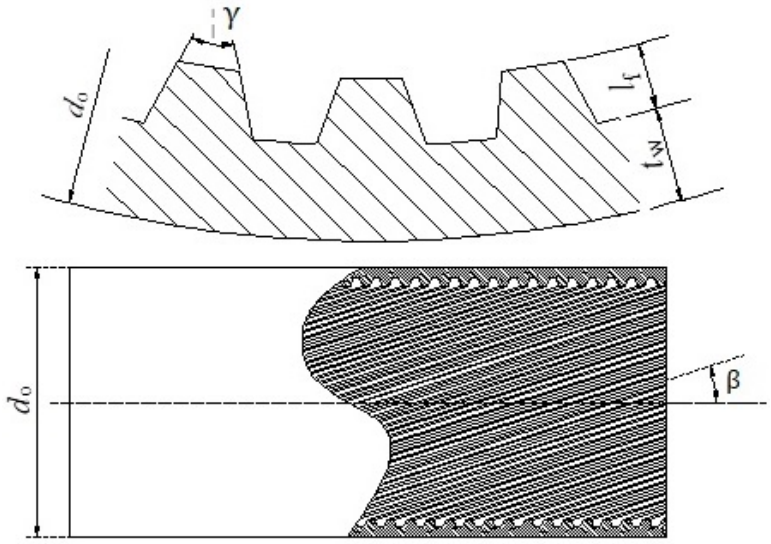

Figure 4. Physical presentation of the geometrical parameters.

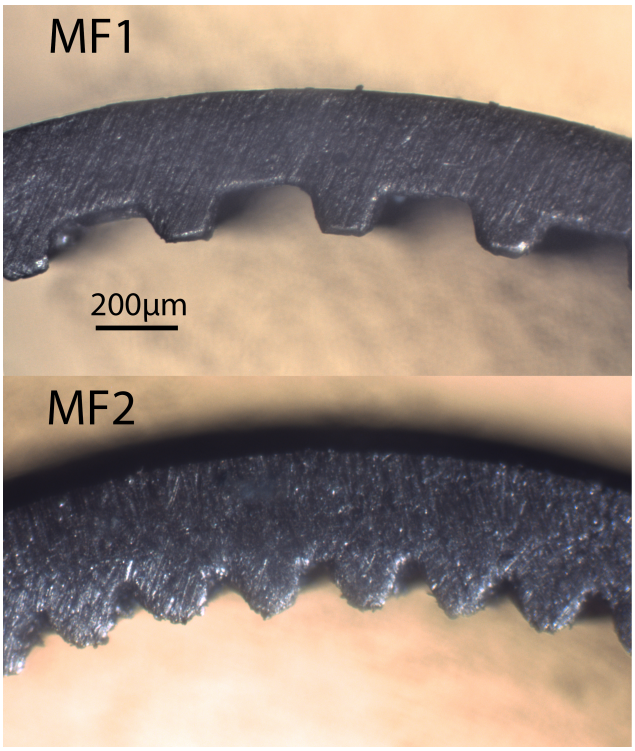

Figure 5. Cross sectional view of the microfinned tubes.

2.2. Working Conditions

Working conditions are summarized in Table 2. Furthermore, the critical fluid properties that seem to have the greatest effect on the two phase flow characteristics are reported.

Table 2. Operating conditions for experimental setup.

	Unit	Range/Value		
		R1270	**R600a**	**R290**
Operating conditions				
Saturation Temperature	°C	35	35	35
Heat flow	W	155	155	155
Mass flux [G]	$kg\,m^{-2}\,s^{-1}$	200–500	200–500	200–500
Vapor quality [x]	-	0.12–0.89	0.13–0.88	0.13–0.84
Quality change [Δx]	-	0.19–0.07	0.18–0.07	0.18–0.07
Fluid properties at 35 °C, Saturated				
Reduced pressure	-	0.32	0.13	0.28
Liquid Viscosity	µPa s	85.7	136.2	87.3
Surface Tension	$mN\,m^{-1}$	5.7	8.9	5.8
Vapor Density	$kg\,m^{-3}$	31.5	12.0	26.6

While no visual observation of flow patterns was performed in this paper, the flow pattern map of Dobson and Chato [23] was used to predict flow regimes. This flow pattern map was compared with experimental results for condensation of propane in Milkie et al. [24] showing good agreement. Interestingly, all the data points tested for smooth tube in this study seem to fall in the annular flow. This is not surprising as, with the small diameter of the tube, surface tension's effect becomes more dominant; furthermore because of charge limitations on the test rig, no tests were performed in really low vapor qualities where the stratified flow occurs. Finally, the mass flow was not high enough to reach mist flow in any of the tested cases. There are flow pattern maps available for the MF tubes [25]. These flow patterns show that microfinned tubes initiate the annular

flow sooner by bringing the liquid from the bottom pool with swirl motion to the top of the tube. Thus, there should be no change in the assumption of all tested points being in annular flow.

2.3. Uncertainty Analysis and Validation

Uncertainty analysis was performed by the method elaborated in ISO [26], and a confidence level exceeding 95% (coverage factor of 2). Utilized instruments and their respective uncertainty are listed in Table 3. The smaller range of absolute pressure sensors for R600a reduces HTC's uncertainty of measurement. The calibration process and formulation used are provided in Appendix A. The average value for uncertainty of measurement of HTC was 6.4%, and this value remains relatively the same in all test conditions. The average uncertainty of measurement for pressure drop was 14.2% with higher values in lower mass fluxes and smooth tubes. In these cases, the pressure drop is small, while the uncertainty of pressure drop measurement based on the full range of the pressure transducer remains the same.

Table 3. List of instruments and their respective uncertainties.

	Type	Range	Uncertainty
Refrigerant Circuit			
Flow meter	Coriolis	0–5 kg min^{-1}	±0.1% [a]
Absolute pressure sensor [c]	Strain gauge	0–10 bar	±0.16% [b]
Absolute pressure sensor [d]	Strain gauge	0–20 bar	±0.16% [b]
Differential pressure sensor	Strain gauge	0–0.5 bar	±0.15% [b]
Thermoucouples	Type T	-	±0.05 K
Preheater	Electrical	3450 W	±0.44% [a]
Cooling Water Circuit			
Flow meter	Coriolis	0–5 kg min^{-1}	±0.1% [a]
RTD	PT 100	-	±0.05 K

[a] Of the reading. [b] Of the set span. [c] Used for R600a. [d] Used for R1270 and R290.

The test rig was validated using a single-phase superheated gas flow of R600a for HTC and R290 for pressure drop in a smooth tube. The Darcy Weisbach formula was used for pressure drop prediction while correlation of Gnielinski V. [27] was used for HTC. The comparison results showed an average absolute deviation of 3.7% and 3.4% for pressure drop and heat transfer coefficient, respectively. To limit the heat leakage to the environment, test sections were insulated using elastomeric foam insulation. Moreover, vacuum heat leakage tests were performed to account for the heat loss to the environment. This was done by flowing water through the helical tube when the test section was under vacuum condition and recording the change in water temperature. This heat loss was taken into account by a linear relationship based on the ambient and test section's surface temperature difference, formulated by Equation (1):

$$Q_{loss} = 0.602 \cdot (T_{element} - T_{amb}) + 0.145 \quad [\mathrm{W}] \tag{1}$$

Heat loss was minimal and in most cases less than 1 W; this is mainly because, with the tested saturation temperature (35 °C), cooling water temperature and subsequently the test section surface temperature were very close to ambient temperature. In several cases, the test section's surface temperature was lower than the ambient temperature, and thus there was heat gain instead of heat loss. This was considered in the data reduction process with a negative value for heat loss.

2.4. Data Reduction

To characterize steady-state condition, the standard deviation of the last 15 samples was calculated; if this value was lower than 0.1 °C, the system was considered to be in

steady-state. The data from the sensors were recorded for over 120 s to obtain 50 samples, which were then averaged. The average vapor quality value is calculated by Equation (2):

$$x = x_{in} - \frac{\Delta x}{2} = \frac{Q_{pre} - \dot{m} \cdot (i_{sat,l} - i_1)}{\dot{m} \cdot i_{\mathrm{lg}(p_{pre})}} - \frac{Q_{test} - Q_{loss}}{2 \cdot \dot{m} \cdot i_{lg(p_{sat})}} \quad (2)$$

i_1 is the enthalpy of subcooled fluid before entering the preheater, p_{pre} is the pressure at the preheater section and p_{sat} is the arithmetic average of the inlet and outlet pressure in the test section. The heat removed from the test section by the cooling water was calculated with Equation (3):

$$Q_{test} = \dot{m}_{water} \cdot c_{P_{water}} \cdot (RTD_2 - RTD_1) \quad (3)$$

Heat transfer coefficient is calculated using Equation (4):

$$HTC = \frac{Q_{test} - Q_{loss}}{S(\overline{T}_{sat} - \overline{T}_w)} \quad (4)$$

where T_{sat} is derived from the saturation pressure, p_{sat}. $\overline{T}_w$ and S are defined as:

$$\overline{T}_w = \frac{1}{4} \sum_{i=1}^{4} T_{w,i} \quad (5)$$

$$S = \pi d_i L \quad (6)$$

The calculation of parameters such as heat flux and mass flux is dependent on the definition of internal diameter d_i. While for the smooth tube this definition is unambiguous, for the MF tube different internal diameters can be defined—namely, fin root diameter, fin tip diameter, and effective diameter, where the effective diameter is the equivalent diameter for a smooth tube with the same actual cross-section area. All three internal diameters for MF tubes are reported in Table 1 but only fin tip diameter was considered for the data reduction process. The reason for this was the simplicity of the measurement process in the field, compatibility with predictive methods and it's conventional use in literature. This choice is critical and should be kept constant across tests. It should be noted that, because of this definition, the values reported for mass flux and heat flux are not the actual values. Nevertheless, the simplicity of measurement and comparison with other correlations outweigh the slight deviation from actual values. The increase in internal area for MF tubes compared to a smooth tube with the same fin tip diameter is calculated using R_x value defined as:

$$R_x = \left\{ \frac{2 \cdot l_f \cdot n \cdot [1 - \sin(\gamma/2)]}{\pi \cdot D \cdot \cos(\gamma/2)} + 1 \right\} \cdot \frac{1}{\cos \beta} \quad (7)$$

This value is not directly used in the data reduction process and thus values such as heat flux for MF tubes are calculated based on a smooth tube with the internal diameter equivalent to fin tip diameter.

Thermodynamic properties are obtained using REFPROP V10 [28]. The total pressure drop Δp is calculated by the addition of momentum pressure drop Δp_a with frictional pressure drop Δp_f. As momentum pressure drop in condensation is negative, it leads to a pressure gain. The void fraction in the momentum pressure drop calculation was determined using Rouhani and Axelsson [29] correlation. This correlation was initially developed for vertical tubes, but it is used here as it has previously reliably calculated data for horizontal tubes.

3. Results and Discussion

3.1. Experimental Data

Figure 6 displays the HTC in the smooth tube for all the the tested fluids at mass fluxes of 200 and 400 kg m^{-2} s^{-1}. The results show that R290 and R1270 have similar behavior in the tested mass fluxes while the HTC of R600a is considerably higher. This can be explained by the thermophysical properties of R600a, specifically, the lower vapor density, which in turn causes a higher superficial velocity of the gas phase, increasing the turbulence at the interface layer between the liquid and gas phase.

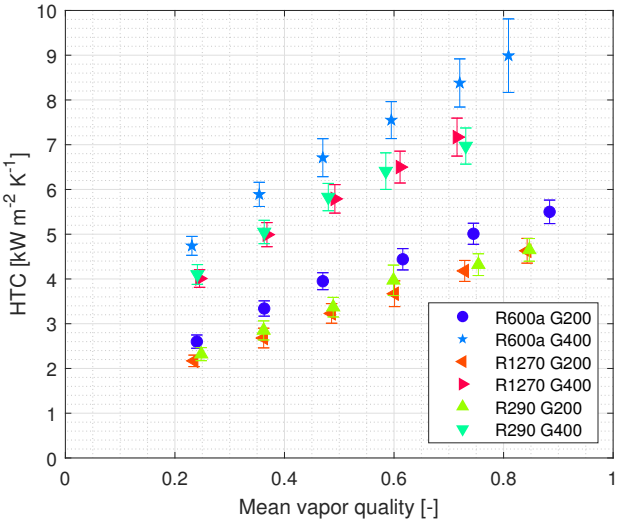

Figure 6. Condensation HTC for R290, R1270, and R600a in smooth tube mass flux (G) reported in kg m^{-2} s^{-1}.

Figure 7 shows how internally enhanced tubes can affect HTC for each of the tested fluids. There is always an increase in the HTC for microfinned tubes compared to the smooth tube. The difference between MF1 and MF2 in R600a is negligible, while, for R290 and R1270, the MF1 tube has a discernibly lower HTC in lower vapor qualities. Thus, it can be said that the higher turbulence caused by higher gas velocity in R600a and at higher vapor qualities diminish the effect of added number of fins and spiral angle in the MF2 tube.

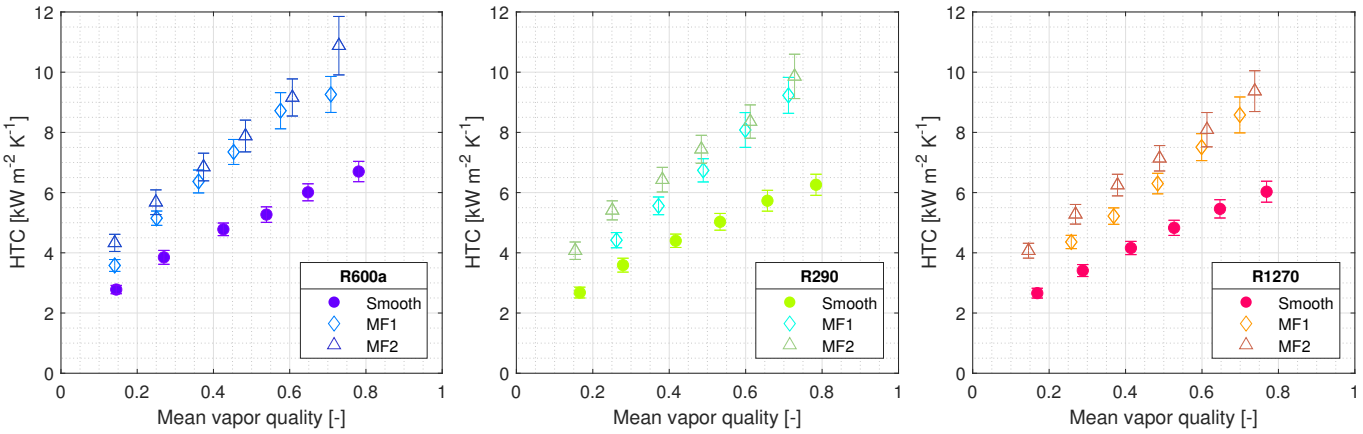

Figure 7. Effect of internal surface enhancement on HTC for R290, R1270, and R600a, G = 300 kg m^{-2} s^{-1}.

Figure 8 shows the effect of microfinned tubes in different mass fluxes and with the different hydrocarbons. In mass flux of 200 kg m^{-2} s^{-1}, the HTC of R600a is distinctly higher than those of R1270 and R290. The differences between HTC of different fluids in

higher mass fluxes are smaller, as the values of MF2 tube with R290 and R1270 reach the values of MF1 with R600a. Interestingly, it seems that, at mass flux of 200 kg m^{-2} s^{-1}, which is the lowest tested mass flux, the trend of HTC with vapor quality is different compared to higher mass fluxes—while, at higher mass fluxes, the HTC values for MF tubes tend to converge because of the lower effect of turbulence created by the surface enhancements; at the lowest mass flux, this trend is diverging. The authors speculate that this is due to the asymmetrical annular flow pattern where the liquid film thickness is higher at the bottom pool. The asymmetrical annular flow pattern assumption is in agreement with [23] where a transitional Froude number is defined for the development of flow regime from wavy-stratified to symmetrical annular flow. In this transitional flow regime, the internal surface enhancement does not create the turbulence needed at the bottom pool of the fluid to make a tangible increase in HTC. At higher vapor qualities, the swirl motion propels the fluid toward a fully developed annular flow, and the turbulence created by the fins differentiates the tubes from each other.

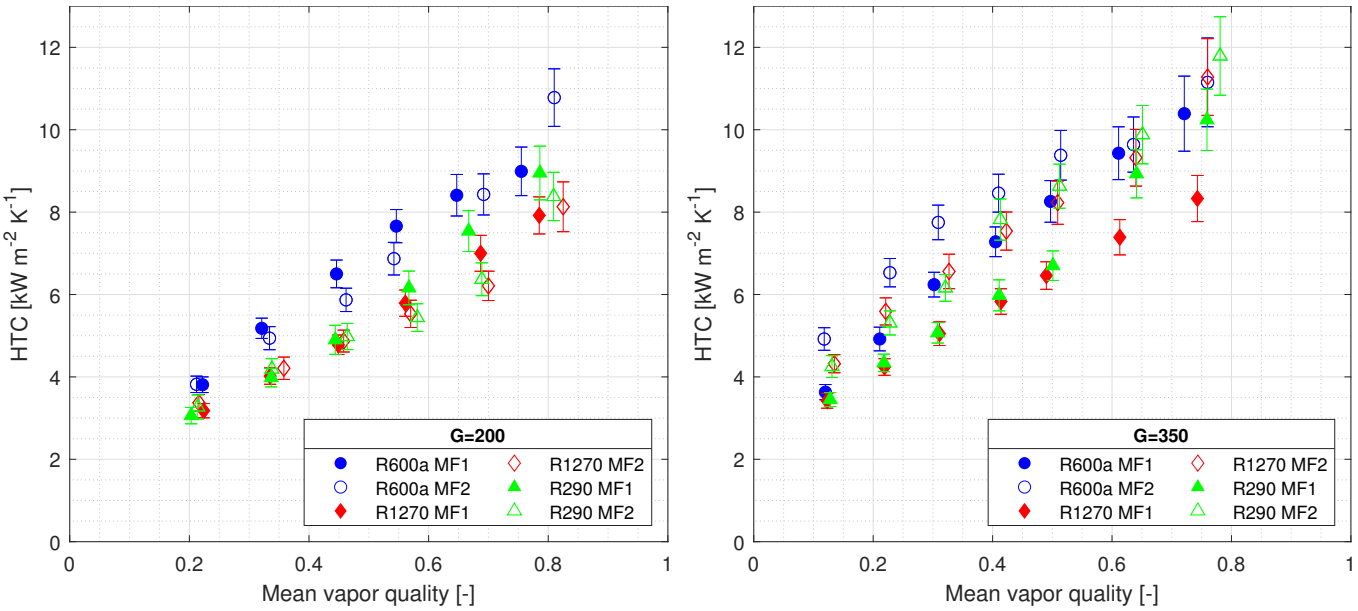

Figure 8. Comparison of HTC in microfinned tubes at different mass fluxes, mass flux (G) reported in the legend in kg m^{-2} s^{-1}.

Figure 9 presents the data for the total pressure gradient. Unsurprisingly, the pressure drop is strongly dependent on the mass flux in all tubes and fluids. Comparing the fluids together, it can be seen that R1270 has a slightly lower pressure drop than R290, while R600a has a significantly higher pressure drop than both other hydrocarbons. Reviewing the Table 2 shows that R600a has a significantly higher liquid viscosity than both of the other fluids; the higher liquid viscosity combined with a lower vapor density of R600a leads to higher shear stress and thus a higher pressure drop. A comparison of microfinned tubes with the smooth tube shows a minor increase for the MF1 tube, while MF2 has a more noticeable increase in pressure drop. To compare the heat transfer and pressure drop characteristics of the microfinned tubes to the smooth tube at the different mass fluxes and vapor qualities, three different parameters were defined. These were Enhancement factor E, Penalization factor P, and efficiency index, I, which are formulated as:

$$E = \frac{HTC_{MF}}{HTC_{Smooth}} \tag{8}$$

$$P = \frac{\Delta p_{MF}}{\Delta p_{Smooth}} \tag{9}$$

$$I = \frac{E}{P} \tag{10}$$

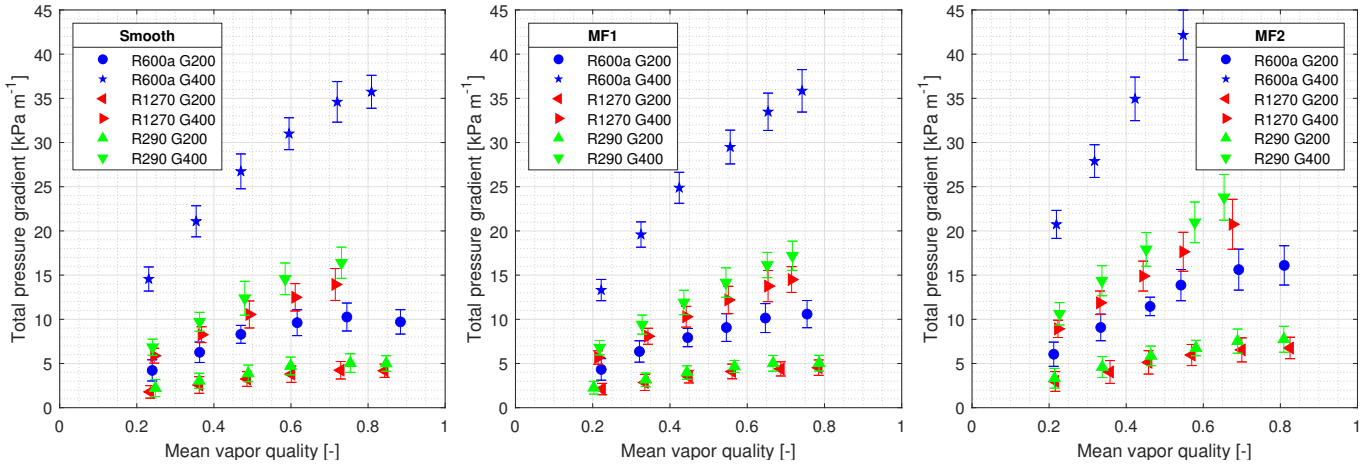

Figure 9. Effect of mass flux on total pressure gradient, mass flux (G) in legend reported in kg m^{-2} s^{-1}.

To distinguish the effect of vapor quality and mass flux, these values were compared at vapor qualities of 0.25 and 0.7 in mass fluxes ranging from 200 to 500 kg m^{-2} s^{-1}. It should be noted that, because of stability issues, not all the data points could be calculated; they mainly lay in the MF2 tube with mass flux of 400 kg m^{-2} s^{-1}. Enhancement factor, E, for both tubes is presented in Figure 10. The MF1 tube has a decreasing enhancement factor with increasing mass flux. Moreover, the enhancement factor is higher at x = 0.7 than x = 0.25. Interestingly, while, at lower mass fluxes, E for both vapor qualities is higher than or close to R_x, as the mass flux increases E falls below R_x meaning that the increase in the internal surface area is not completely utilized. This is more apparent for the MF2 tube where E is more or less uniform regardless of fluid or vapor quality and much lower than R_x. These results can be explained by arguing that fins have a twofold effect on flow. First, the fins can agitate the boundary layer at the wall, providing more turbulence and thus removing more heat; this seems to be the dominating contributor at lower mass fluxes. Secondly, the fins provide extra heat transfer area; this is more apparent in higher mass fluxes where the boundary layer is already agitated and the extra turbulence created by fins is not a significant contributing factor.

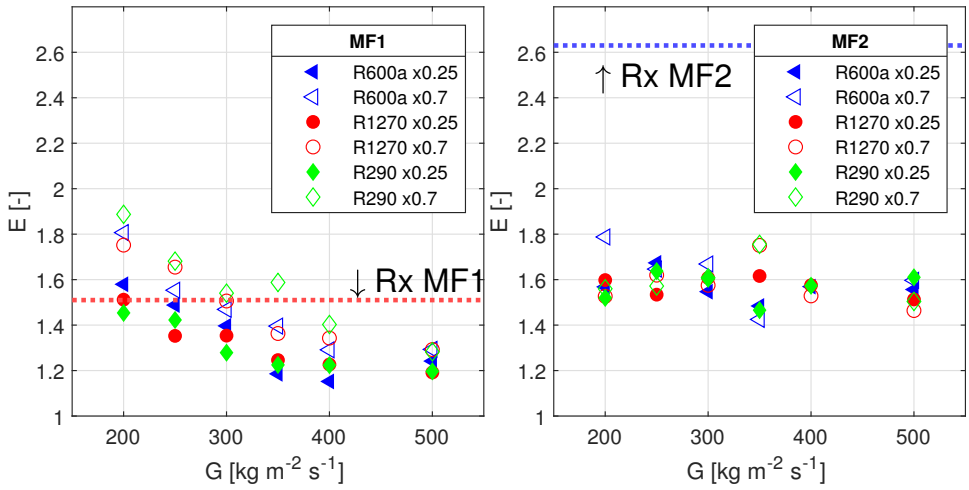

Figure 10. Effect of mass flux on enhancement factor, E, for MF tubes at x = 0.25 and x = 0.7, heat exchange area increase shown with R_x.

Figure 11 displays the penalization factor, P. Both tubes seem to present more or less stable values for P regardless of the tested fluid and the vapor quality, although MF2 shows more scatter in the data. Nevertheless, it can be observed that the penalization factor is far higher for MF2 tube than MF1. This was to be expected considering the higher fin number and spiral angle of the MF2 tube. Furthermore, P does not seem to be a function of mass flux, even if it is the most defining factor for pressure drop.

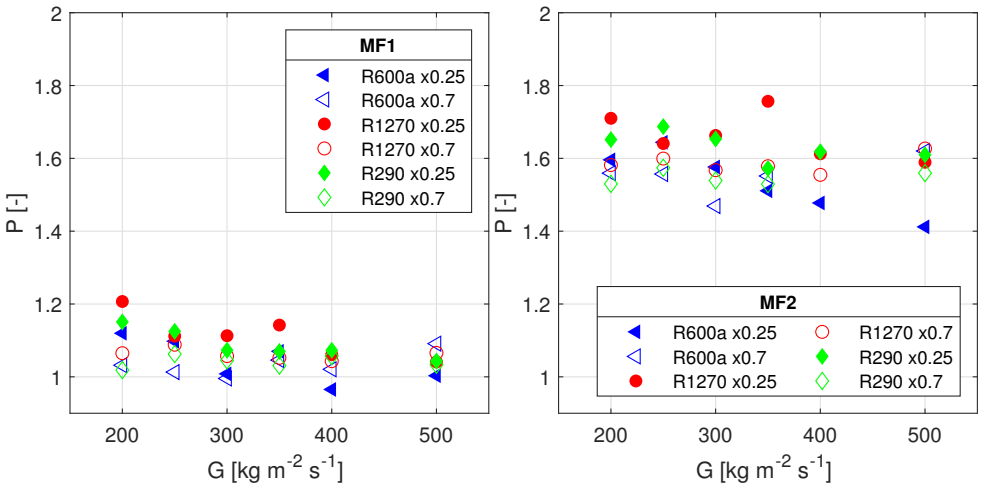

Figure 11. Effect of mass flux on penalization factor, P, for MF tubes at x = 0.25 and x = 0.7.

Finally, the efficiency index, I, is shown in Figure 12. The MF1 tube seems to be more advantageous in higher vapor qualities with values reaching more than 1.8; this was expected since E is decreasing while P is stable. R600a seems to enjoy a slightly better I value at x = 0.25 in low mass fluxes, while, at other conditions, the results are mostly independent of the tested fluid. As for MF2, it can be seen that the results are largely uniform across the fluids, mass fluxes and vapor qualities. More importantly, I is close to 1 and significantly lower than MF1 for most tested cases. This means that the increase in pressure drop offsets the increase in HTC. If the efficiency index was to be considered a measure of how beneficial an internally enhanced tube is, it could be argued that, with an efficiency index of unity, there is no difference in employing MF2 tube compared to a smooth tube. This is not considering other factors in the design of a heat exchanger such as the extra cost in the production of this tube, header size, or air side resistance. However, if the heat exchanger design goal is to minimize the charge in the system, MF2 provides additional benefits as it provides a higher HTC, especially as this increase is uniform across the vapor qualities. This is important as it seems that the MF1 tube has a lower E for lower vapor qualities where the majority of charge is located. Hence, heat exchangers can be designed with MF2 tube that have a shorter length for lower vapor qualities, thus reducing the charge significantly.

3.2. Correlations

Applicable predictive methods were compared against HTC and pressure drop experimental data in all tested conditions utilizing Mean Relative Deviation (MRD) and Mean Absolute Relative Deviation (MARD), defined as:

$$MRD = \frac{100}{N}\sum_{i=1}^{N}\frac{Predicted_i - Experimental_i}{Experimental_i} \tag{11}$$

$$MARD = \frac{100}{N}\sum_{i=1}^{N}\left|\frac{Predicted_i - Experimental_i}{Experimental_i}\right| \tag{12}$$

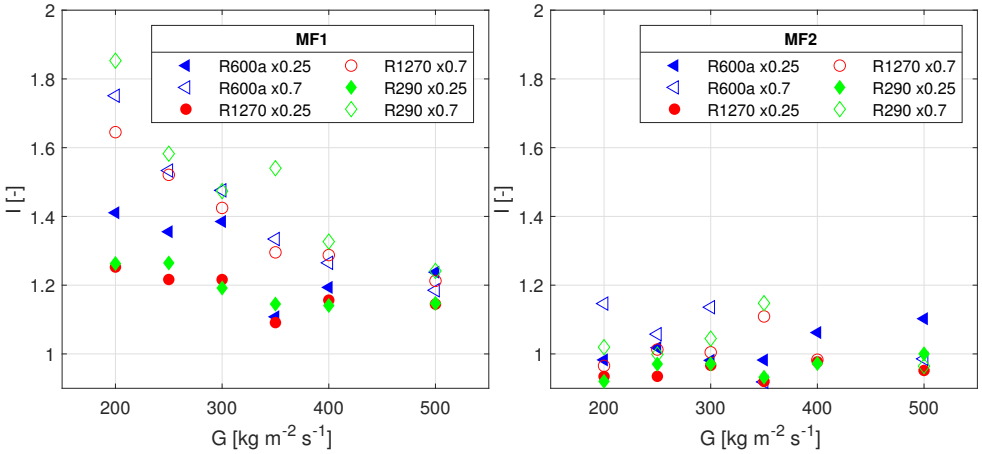

Figure 12. Effect of mass flux on efficiency index, I, for MF tubes at x = 0.25 and x = 0.7.

Furthermore, δ_{30} is defined as the percentage of the predicted values having less than 30% deviation from the experimental data. The correlations were chosen on the basis of the database they were developed with, such as Macdonald and Garimella [9] that considered condensation of hydrocarbons, or Xu and Fang [30] that uses Weber number to take into account surface tension that is important in compact tubes. Table 4 summarizes the results of comparison for both of the fluids in smooth tube.

Table 4. Comparison between experimental results and correlations for HTC and pressure drop in smooth tube, with best performing correlations in bold.

	R600a			**R1270**			**R290**		
	MRD %	**MARD%**	δ_{30}	**MRD %**	**MARD%**	δ_{30}	**MRD %**	**MARD%**	δ_{30}
Pressure Drop Correlations									
Müller-Steinhagen and Heck [31]	−18.4	19.0	97.4	−14.1	14.9	100	−16.2	16.7	100
Cavallini et al. [32]	2.0	11.6	94.7	−14.5	17.6	100	−13.0	16.1	97.3
Macdonald and Garimella [9]	10.9	14.0	97.4	**−6.1**	**6.4**	**100**	**−7.8**	**7.9**	**100**
Xu and Fang [30]	**−6.5**	**11.0**	**100**	−3.2	9.4	100	−4.6	10.1	100
Friedel [33]	−18.3	19.0	100	−5.5	9.3	100	−9.3	11.7	100
HTC Correlations									
Macdonald and Garimella [9]	−21.9	21.9	89.5	−23.5	23.5	81.1	−25.3	25.3	67.6
Shah [34]	18.6	18.6	97.4	24.3	33.4	24.3	28.4	28.4	62.2
Dorao and Fernandino [35]	**−5.0**	**5.8**	**100**	**11.0**	**11.0**	**100**	**4.9**	**4.9**	**100**

All of the correlations chosen for prediction of pressure drop performed reasonably well, with correlations of Macdonald and Garimella [9] and Xu and Fang [30] providing slightly more accurate results. Thus, any of these correlations could be used for reliable prediction of the pressure of hydrocarbons in smooth tubes. As for HTC correlations, it seems that, while Macdonald and Garimella [9] and Shah [34] can be reasonably accurate for R600a, their error increases for other tested hydrocarbons. The most accurate correlation was Dorao and Fernandino [35] in which authors have proposed a correlation where the two-phase HTC is substituted with an analogous single phase flow HTC. This correlation was able to predict all HTC data points for all fluids with less than 30% error; this is shown as a parity plot in Figure 13. In addition to being accurate, this correlation is much simpler to implement than other correlations where parameters such as liquid film thickness must be calculated.

It should be noted that, for microfinned tubes, the formulation and parameter definition in each paper was used, i.e., the formulation and parameters in this study were adapted accordingly to match the correlation's definition.

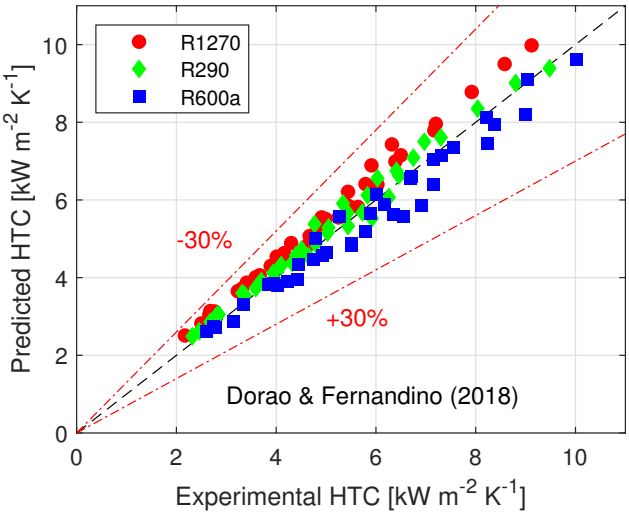

Figure 13. Comparison between experimental data and correlations of Dorao and Fernandino [35] for prediction of HTC in smooth tubes.

Table 5 compares the prediction methods for pressure drop with experimental data in microfinned tubes. As the tube's geometry has a notable effect on pressure drop characteristics, the data for each tube are reported separately. In the MF1 tube, correlation of Diani et al. [36] reliably predicts pressure drop for all fluids, the same correlation can predict pressure drop values in MF2 tube as well, albeit with a relatively higher error. Correlation of Choi et al. [37] underpredicts the MF1 pressure drop values but has the lowest MARD for R290 and R1270 in MF2. In general, the Diani et al. [36] correlation provides a reliable and safe method to predict pressure drop with an acceptable level of error in evaporation flow as well as condensation flow Allymehr et al. [21,22].

Table 5. Comparison between experimental data and correlations for prediction of pressure drop in microfinned tubes, with best performing correlations highlighted in bold.

	R600a			**R1270**			**R290**		
	MRD %	**MARD%**	δ_{30}	**MRD %**	**MARD%**	δ_{30}	**MRD %**	**MARD%**	δ_{30}
MF1 tube									
Rollmann and Spindler [38]	14.6	14.6	97.4	12.2	14.0	91.9	12.1	13.5	94.6
Choi et al. [37]	−29.5	29.5	52.6	−32.0	32.0	45.9	−32.1	32.1	43.2
Diani et al. [36]	**12.8**	**12.8**	**94.7**	**5.7**	**8.1**	**97.3**	**−7.3**	**5.4**	**97.3**
MF2 tube									
Rollmann and Spindler [38]	−26.1	26.1	75.0	-28.5	28.5	59.5	−28.7	28.7	59.5
Choi et al. [37]	14.1	17.0	88.9	**8.1**	**11.7**	**100**	**8.0**	**11.8**	**100**
Diani et al. [36]	**−16.7**	**16.7**	**100**	−22.2	22.2	94.6	−22.1	22.1	100

Comparison of the experimental data with HTC correlations of microfinned tubes is reported in Table 6. Cavallini et al. [39] accurately predicts the data for all fluids in the MF1 tube. The results for MF2 tube are mixed, and, in general, correlations cannot predict the results as accurately as with MF1. This is expected as the MF2 tube has a novel geometry with a higher number of fins and spiral angle, and this geometry has not been widely studied for two-phase flow characteristics and thus incorporated in the correlations database. Cavallini et al. [39] seems to underestimate HTC considerably. A closer look at the correlation reveals that authors have considered a term to lower the effect of microfinned in the forced convective condensation term if the number of fins is deemed higher than an optimum level. This condition applies to the MF2 tube and, based on the results in this paper, is a reasonable assumption to make. A simple change

in the values proposed for the equation of reducing term enables the correlation to fit the experimental results. As the MF2 tube was the only tube that needed the reduction term to be calculated, the authors cannot advise this method as a revised formulation of Cavallini et al. [39] correlation.

Table 6. Comparison between experimental data and correlations for prediction of HTC in microfinned tubes, with best correlations highlighted in bold.

	R600a			R1270			R290		
	MRD %	**MARD%**	δ_{30}	**MRD %**	**MARD%**	δ_{30}	**MRD %**	**MARD%**	δ_{30}
MF1 tube									
Cavallini et al. [39]	**5.5**	**7.8**	**100**	**12.3**	**13.6**	**100**	**5.2**	**7.9**	**100**
Yu and Koyama [40]	52.6	52.6	18.4	46.2	46.2	13.5	40.5	40.5	32.4
Kedzierski and Goncalves [41]	−25.7	25.7	89.5	−18.2	18.2	97.3	−24.5	24.5	89.2
MF2 tube									
Cavallini et al. [39]	−41.5	41.5	0	−39.1	39.1	13.5	−42.0	42.0	5.4
Yu and Koyama [40]	33.8	33.8	50.0	**25.6**	**25.6**	**67.6**	**23.0**	**23.0**	**78.4**
Kedzierski and Goncalves [41]	**−32.2**	**32.2**	**44.4**	−26.6	26.6	54.1	−31.1	31.1	37.8

This study's goal was not to develop a new correlation and the data in this paper clearly indicate that the extra heat exchange area is not the only parameter affecting the heat transfer characteristics. However, for a back-of-the-envelope calculation for HTC, the authors suggest using correlations developed for smooth tubes and multiplying them by the increased area with a reducing term for highly finned tubes. A quick calculation showed that, considering this method with Dorao and Fernandino [35] for MF1, most data points can be calculated with less than 30% error while grossly over-predicting HTC in MF2 tube. An analysis of the effect of various internal surface enhancements on HTC can help develop a better reduction term and simplify the prediction of HTC in microfinned tubes.

The accuracy of Kedzierski and Goncalves [41] and Cavallini et al. [39] for both MF tubes is visualized in Figure 14. Cavallini et al. [39] can follow MF1 data accurately while MF2 data are underpredicted, and this error is slightly higher for R290. On the other hand, while the correlation of Kedzierski and Goncalves [41] underpredicts HTC values for both MF1 and MF2, this under prediction is rather constant at around 30% suggesting an offset problem.

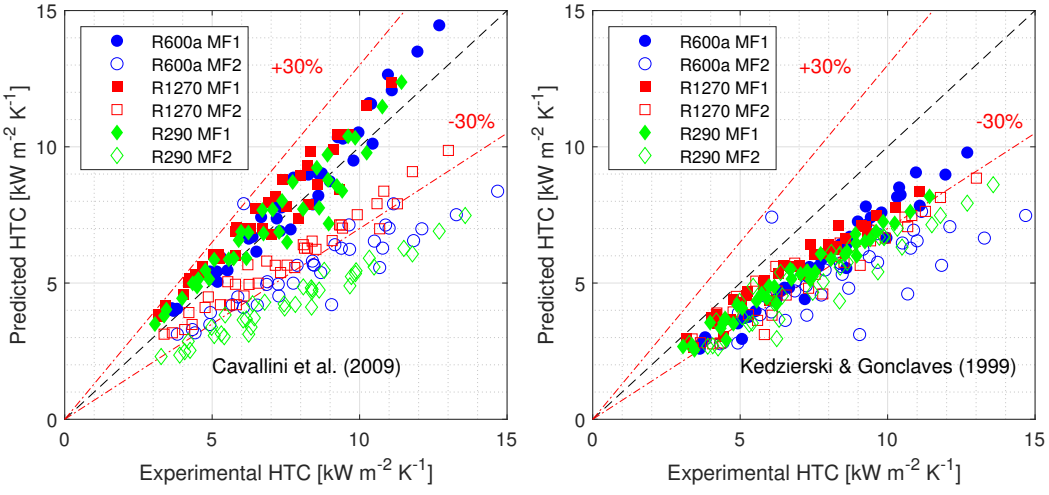

Figure 14. Prediction of HTC in two microfinned tubes by correlations of Cavallini et al. [39] and Kedzierski and Goncalves [41] compared to experimental data.

4. Conclusions

Internally enhanced tubes offer the possibility of a more efficient and smaller heat exchanger, providing a higher capacity with a reduced charge. The lack of data for elements such as heat transfer coefficient and pressure drop makes the design process of these heat exchangers challenging, especially for hydrocarbons where the amount of charge is critical. This paper tries to address this problem by reporting experimental results on the condensation flow characteristics of three hydrocarbons, namely, propane (R290), isobutane (R600a), and propylene (R1270). Three tubes with an outer diameter of 5 mm were tested, one smooth tube and two microfinned tubes with an increased heat exchange area of 1.51 and 2.63 for MF1 and MF2, respectively. Experimental tests were performed at saturation temperatures 35 °C and mass fluxes from 200 to 500 kg m^{-2} s^{-1}.

The results are critically compared, noting the effect of surface enhancements and different fluids. Data obtained show that mass flux strongly affects HTC and pressure drop. R600a has a higher HTC and pressure drop mainly because of its lower vapor density, while the characteristics of R1270 and R290 seem to be very close.

The microfinned tubes behave differently; MF1 tube increases the HTC coefficient more in lower mass fluxes and higher vapor qualities, while the MF2 tube has a relatively constant increase in the HTC in all vapor qualities and mass fluxes. The increase of HTC for both tubes seems to be independent of fluid tested. The maximum increase of HTC for MF1 tube reached up to 1.8 while the increase of HTC for MF2 mainly is around 1.6. It can be deduced that the increase in the number of fins and heat exchange area have a diminishing return on the HTC capabilities of an internally enhanced tube. The increase of pressure drop between smooth and internally enhanced tubes was relatively constant for all the fluids, mass fluxes, and vapor qualities, being around 1.2 for MF1 and significantly higher, at around 1.7, for MF2 tube. All in all, for the MF1 tube with an increase in mass flux, the pressure drop increases stay the same, while the increase in HTC decreases, discouraging its use in higher mass fluxes. The MF2 tube seems to have the same effectiveness at all mass fluxes but at a lower level than MF1. A more detailed evaluation of some of these results and trends, including potential instabilities, dryout and flow patterns, is not possible with the current design of the test section and sight glass available. The unit is being upgraded with a fitting sight glass and high-speed camera to allow the next step in this research line by flow visualization of two-phase hydrocarbon flow in compact, smooth, and microfinned tubes. The comparison of experimental data with predictive methods shows that the HTC and pressure drop in the smooth tube are reliably predicted by Dorao and Fernandino [35] and Macdonald and Garimella [9], respectively. For microfinned tubes, Diani et al. [36] predicted pressure drop data for both MF1 and MF2 tube. As for HTC in microfinned tubes, the accuracy of the prediction methods varied based on the tested tube, with the data of MF1 being accurately predicted by Cavallini et al. [42] for all fluids. No reliable equations were found for HTC prediction in the MF2 tube.

Author Contributions: Conceptualization, E.A., A.H., T.M.E., and Á.Á.P.; methodology, E.A and Á.Á.P.; software, E.A.; validation, E.A.; formal analysis, E.A. and Á.Á.P.; investigation, E.A. and Á.Á.P.; resources, A.H. and T.M.E.; data curation, E.A. and Á.Á.P.; writing—original draft preparation, E.A. and Á.Á.P.; writing—review and editing, E.A. and Á.Á.P.; visualization, E.A.; supervision, A.H. and T.M.E.; project administration, A.H. and T.M.E.; funding acquisition, A.H., T.M.E. All authors have read and agreed to the published version of the manuscript.

Funding: This publication has been funded by HighEFF—Centre for an Energy Efficient and Competitive Industry for the Future, an 8-year Research Centre under the FME-scheme (Centre for Environment-friendly Energy Research, 257632). The authors gratefully acknowledge the financial support from the Research Council of Norway and user partners of HighEFF.

Institutional Review Board Statement: Not applicable.

Informed Consent Statement: Not applicable.

Conflicts of Interest: The authors declare no conflict of interest.

Abbreviations

Greek

β	Spiral angle
δ_{30}	Percentage of predicted values with less than 30% error
γ	Fin angle

Roman

$c_{P_{water}}$	Specific heat of water [J g^{-1} K^{-1}]
d_i	Fin tip diameter for MF tubes, internal diameter for smooth tube [mm]
d_o	Outer diameter [mm]
E	Enhancement Factor [-]
G	Mass flux [kg m^{-2} s^{-1}]
HTC	Heat Transfer Coefficient [kW m^{-2} K^{-1}]
I	Efficiency index [-]
i_{lg}	Enthalpy of vaporization [kJ kg^{-1}]
l_f	Fin height [mm]
m	Mass flow [kg s^{-1}]
$MARD$	Mean Absolute Relative Deviation [-]
MRD	Mean Relative Deviation [-]
N	Dataset size [-]
n	Number of fins [-]
P	Penalization Factor [-]
p	Pressure [Pa]
P_r	Reduced pressure [-]
Q	Heat input [W]
q	Heat flux [kW m^{-2}]
R_x	Heat exchange area ratio to a smooth tube [-]
RTD	Resistance thermometers [-]
S	Heat exchange area [m^2]
T	Temperature [°C]
t_w	Wall thickness [mm]
x	Vapor quality [-]

Subscripts

a	Advectional
amb	Ambient condition
$element$	Heating Element
f	Frictional
in	Inlet conditions
l	Liquid phase
lg	Liquid to gas phase change
$loss$	Heat loss to environment
pre	Preheater section
sat	Saturated condition
$test$	Test section
w	Wall

Appendix A. Calibration Process and Uncertainty Propagation

In order to calibrate the thermocouples, AMETEK JOFRA RTC 157 Reference Temperature Calibrator with the procedure advised by the manufacturer has been used. This unit has an accuracy of ±0.04 °C and stability of ±0.005 °C. The thermocouples were connected in the same manner as the testing condition (same cables, connections, DAQ) and the values were read each five degrees in the desired temperature range (−10 °C to 30 °C). The same procedure was used to calibrate the RTD elements in a temperature range of −20 to 70 °C. The obtained data from the calibration process were used to create a calibration file in LabVIEW.

Below, the formulation used for propagating of uncertainty is summarized. Uncertainty for wall temperature:

$$u(T_w) = \sqrt{(1/4)^2 \cdot \sum_{i=4}^{7} u(T_i)} \tag{A1}$$

Uncertainty for Saturation temperature:

$$u(T_{sat}) = \sqrt{(\frac{\partial T_{sat}}{\partial P_{sat}})^2 \cdot u(p_{sat})^2} \tag{A2}$$

From the Antoine equation, the relationship between saturation temperature and saturation pressure can be found; by derivation, it can be written:

$$(\frac{\partial T_{sat}}{\partial P_{sat}}) = \frac{803.99}{P_{sat} \cdot (3.9228 - \log_{10}(P_{sat}))} \tag{A3}$$

Uncertainty for heat transfer coefficient:

$$u(h) = \sqrt{\left(\frac{u(Q_{test})}{T_{\mathrm{w}} - T_{\mathrm{sat}}}\right)^2 + \left(\frac{Q_{test} \cdot u(T_{\mathrm{w}})}{(T_{\mathrm{w}} - T_{\mathrm{sat}})^2}\right)^2 + \left(\frac{Q_{test} \cdot u(T_{\mathrm{sat}})}{(T_{\mathrm{w}} - T_{\mathrm{sat}})^2}\right)^2} \tag{A4}$$

where the uncertainty of the heat input is calculated as:

$$u(Q_{test}) = \sqrt{(u(\dot{m}_{water}) \cdot c_{P_{water}} \cdot (RTD_2 - RTD_1))^2 + (\dot{m}_{water} \cdot c_{P_{water}})^2 \cdot (u(RTD_1)^2 + u(RTD_2)^2))} \tag{A5}$$

Uncertainty for inlet vapor quality:

$$u(x_{in}) = \sqrt{\left(\frac{u(Q_{pre})}{\dot{m} \cdot i_{lg(P1)}}\right)^2 + \left(\frac{Q_{pre} \cdot u(\dot{m})}{i_{lg(P1)} \cdot \dot{m}^2}\right)^2} \tag{A6}$$

Uncertainty for the change in vapor quality:

$$u(\Delta x) = \sqrt{\left(\frac{u(Q_{test})}{\dot{m} \cdot i_{lg(P_{sat})}}\right)^2 + \left(\frac{Q_{test} \cdot ln(\dot{m}) \cdot u(\dot{m})}{i_{lg(P_{sat})}}\right)^2} \tag{A7}$$

Uncertainty for the average vapor quality:

$$u(x) = \sqrt{u(x_{in}) + 1/4 \cdot u(\Delta x)^2} \tag{A8}$$

References

1. Straub, M. Alternative Refrigerants For Household Refrigerators. In *International Refrigeration and Air Conditioning*; Purdue University: West Lafayette, IN, USA, 2018; Volume 2002, pp. 1–10.
2. Tang, W.; He, G.; Zhou, S.; Sun, W.; Cai, D.; Mei, K. The performance and risk assessment of R290 in a 13 kW air source heat pump. *Appl. Therm. Eng.* **2018**, *144*, 392–402. [CrossRef]
3. Palm, B. Hydrocarbons as refrigerants in small heat pump and refrigeration systems—A review. *Int. J. Refrig.* **2008**, *31*, 552–563. [CrossRef]
4. Li, T.; Lu, J.; Chen, L.; He, D.; Qiu, X.; Li, H.; Liu, Z. Measurement of refrigerant mass distribution within a R290 split air conditioner. *Int. J. Refrig.* **2015**, *57*, 163–172. [CrossRef]
5. Thonon, B. A review of hydrocarbon two-phase heat transfer in compact heat exchangers and enhanced geometries. *Int. J. Refrig.* **2008**, *31*, 633–642. [CrossRef]

6. Moreira, T.A.; Furlan, G.; e Oliveira, G.H.D.S.; Ribatski, G. Flow boiling and convective condensation of hydrocarbons: A state-of-the-art literature review. *Appl. Therm. Eng.* **2021**, *182*, 116129. [CrossRef]
7. Nan, X.H.; Infante Ferreira, C. In tube evaporation and condensation of natural refrigrant R290 (Propane). In Proceedings of the Gustav Lorentz Conference, Purdue, IN, USA, 25–28 July 2000; Volume 290, p. 3.
8. Macdonald, M.; Garimella, S. Hydrocarbon condensation in horizontal smooth tubes: Part I—Measurements. *Int. J. Heat Mass Transf.* **2016**, *93*, 75–85. [CrossRef]
9. Macdonald, M.; Garimella, S. Hydrocarbon condensation in horizontal smooth tubes: Part II—Heat transfer coefficient and pressure drop modeling. *Int. J. Heat Mass Transf.* **2016**, *93*, 1248–1261. [CrossRef]
10. Lee, H.S.; Yoon, J.I.; Kim, J.D.; Bansal, P. Condensing heat transfer and pressure drop characteristics of hydrocarbon refrigerants. *Int. J. Heat Mass Transf.* **2006**, *49*, 1922–1927. [CrossRef]
11. Del Col, D.; Stefano, B.; Matteo, B.; Luisa, R. Condensation Heat Transfer and Pressure Drop with Propane in a Minichannel. In Proceedings of the International Refrigeration and Air Conditioning Conference, West Lafayette, IN, USA, 16–19 July 2012.
12. Ağra, Ö.; Teke, İ. Experimental investigation of condensation of hydrocarbon refrigerants (R600a) in a horizontal smooth tube. *Int. Commun. Heat Mass Transf.* **2008**, *35*, 1165–1171. [CrossRef]
13. Qiu, G.; Li, M.; Cai, W. The condensation heat transfer, frictional pressure drop and refrigerant charge characteristics of R290 in minichannels with different diameters. *Int. J. Heat Mass Transf.* **2020**, *158*, 119966. [CrossRef]
14. Wen, J.; Gu, X.; Wang, S.; Li, Y.; Tu, J. The comparison of condensation heat transfer and frictional pressure drop of R1234ze(E), propane and R134a in a horizontal mini-channel. *Int. J. Refrig.* **2018**, *92*, 208–224. [CrossRef]
15. Longo, G.A.; Mancin, S.; Righetti, G.; Zilio, C. Saturated vapour condensation of HFC404A inside a 4 mm ID horizontal smooth tube: Comparison with the long-term low GWP substitutes HC290 (Propane) and HC1270 (Propylene). *Int. J. Heat Mass Transf.* **2017**, *108*, 2088–2099. [CrossRef]
16. Longo, G.A.; Mancin, S.; Righetti, G.; Zilio, C. Saturated vapor condensation of hydrocarbons inside A 4 mm ID horizontal smooth tube. *Refrig. Sci. Technol.* **2018**, *2018*, 620–627. [CrossRef]
17. Colombo, L.; Lucchini, A.; Muzzio, A. Flow patterns, heat transfer and pressure drop for evaporation and condensation of R134A in microfin tubes. *Int. J. Refrig.* **2012**, *35*, 2150–2165. [CrossRef]
18. Bashar, M.K.; Nakamura, K.; Kariya, K.; Miyara, A. Condensation heat transfer of R1234yf in a small diameter smooth and microfin tube and development of correlation. *Int. J. Refrig.* **2020**, *120*, 331–339. [CrossRef]
19. Diani, A.; Brunello, P.; Rossetto, L. R513A condensation heat transfer inside tubes: Microfin tube vs. smooth tube. *Int. J. Heat Mass Transf.* **2020**, *152*, 119472. [CrossRef]
20. Han, D.; Lee, K.J. Experimental study on condensation heat transfer enhancement and pressure drop penalty factors in four microfin tubes. *Int. J. Heat Mass Transf.* **2005**, *48*, 3804–3816. [CrossRef]
21. Allymehr, E.; Pardiñas, Á.Á.Á.; Eikevik, T.M.T.; Hafner, A. Comparative analysis of evaporation of Isobutane (R600a) and Propylene (R1270) in compact smooth and microfinned tubes. *Appl. Therm. Eng.* **2021**, *188*, 116606. [CrossRef]
22. Allymehr, E.; Pardiñas, Á.Á.; Eikevik, T.M.; Hafner, A. Characteristics of evaporation of propane (R290) in compact smooth and microfinned tubes. *Appl. Therm. Eng.* **2020**, *181*, 115880. [CrossRef]
23. Dobson, M.K.; Chato, J.C. Condensation in smooth horizontal tubes. *J. Heat Transf.* **1998**, *120*, 193–213. [CrossRef]
24. Milkie, J.A.; Garimella, S.; Macdonald, M.P. Flow regimes and void fractions during condensation of hydrocarbons in horizontal smooth tubes. *Int. J. Heat Mass Transf.* **2016**, *92*, 252–267. [CrossRef]
25. Rollmann, P.; Spindler, K. A new flow pattern map for flow boiling in microfin tubes. *Int. J. Multiph. Flow* **2015**, *72*, 181–187. [CrossRef]
26. ISO. Guide to Expression of Uncertainty in Measurement. 1993. Available online: https://www.bipm.org/documents/20126/2071204/JCGM_100_2008_E.pdf/cb0ef43f-baa5-11cf-3f85-4dcd86f77bd6 (accessed on 5 May 2021).
27. Gnielinski, V. New equations for heat and mass transfer in the turbulent flow in pipes and channels. *Forsch. Ingenieurwesen* **1975**, *41*, 8–16. [CrossRef]
28. Lemmon, E.W.; Bell, I.H.; Huber, M.L.; McLinden, M.O. NIST Standard Reference Database 23: Reference Fluid Thermodynamic and Transport Properties-REFPROP. Version 10.0. National Institute of Standards and Technology. Available online: https://tsapps.nist.gov/publication/get_pdf.cfm?pub_id=912382 (accessed on 5 May 2021).
29. Rouhani, S.Z.; Axelsson, E. Calculation of void volume fraction in the subcooled and quality boiling regions. *Int. J. Heat Mass Transf.* **1970**, *13*, 383–393. [CrossRef]
30. Xu, Y.; Fang, X. A new correlation of two-phase frictional pressure drop for condensing flow in pipes. *Nucl. Eng. Des.* **2013**, *263*, 87–96. [CrossRef]
31. Müller-Steinhagen, H.; Heck, K. A simple friction pressure drop correlation for two-phase flow in pipes. *Chem. Eng. Process. Process. Intensif.* **1986**, *20*, 297–308. [CrossRef]
32. Cavallini, A.; Censi, G.; Col, D.D.; Doretti, L.; Longo, G.; Rossetto, L. Condensation of Halogenated Refrigerants Inside Smooth Tubes. *HVAC&R Res.* **2002**, *8*, 429–451. [CrossRef]
33. Friedel, L. Improved friction pressure drop correlation for horizontal and vertical two-phase pipe flow. In Proceedings of the European Two-Phase Flow Group Meeting, Ispra, VA, Italy, 5–7 June 1979; pp. 485–492.
34. Shah, M.M. An Improved and Extended General Correlation for Heat Transfer during Condensation in Plain Tubes. *HVAC&R Res.* **2009**, *15*, 889–913. [CrossRef]

35. Dorao, C.A.; Fernandino, M. Simple and general correlation for heat transfer during flow condensation inside plain pipes. *Int. J. Heat Mass Transf.* **2018**, *122*, 290–305. [CrossRef]
36. Diani, A.; Mancin, S.; Rossetto, L. R1234ze(E) flow boiling inside a 3.4 mm ID microfin tube. *Int. J. Refrig.* **2014**, *47*, 105–119. [CrossRef]
37. Choi, J.Y.; Kedzierski, M.A.; Domanski, P.A. Generalized Pressure Drop Correlation for Evaporation and Condensation in Smooth and Micro-Fin Tubes. In Proceedings of the IIF-IIR-Commission B1, Paderborn, Germany, 2–5 October 2001.
38. Rollmann, P.; Spindler, K. New models for heat transfer and pressure drop during flow boiling of R407C and R410A in a horizontal microfin tube. *Int. J. Therm. Sci.* **2016**, *103*, 57–66. [CrossRef]
39. Cavallini, A.; Del Col, D.; Mancin, S.; Rossetto, L. Condensation of pure and near-azeotropic refrigerants in microfin tubes: A new computational procedure. *Int. J. Refrig.* **2009**, *32*, 162–174. [CrossRef]
40. Yu, J.; Koyama, S. Condensation heat transfer of pure refrigerants in microfin tubes. In Proceedings of the International Refrigeration and Air Conditioning Conference, West Lafayette, IN, USA, 14–17 July 1998.
41. Kedzierski, M.A.; Goncalves, J.M. Horizontal Convective Condensation of Alternative Refrigerants Within a Micro-Fin Tube. *J. Enhanc. Heat Transf.* **1999**, *6*, 161–178. [CrossRef]
42. Cavallini, A.; Del Col, D.; Matkovic, M.; Rossetto, L. Pressure drop during two-phase flow of R134a and R32 in a single Minichannel. *J. Heat Transf.* **2009**, *131*, 1–8. [CrossRef]